Anatomy of charge-exchange straggling

Sigmund, Peter; Osmani, Orkhan; Schinner, Andreas

Published in:
Nuclear Instruments and Methods in Physics Research Section B: Beam Interactions with Materials and Atoms

DOI:
10.1016/j.nimb.2014.08.006

Publication date:
2014

Document version:
Submitted manuscript

Citation for pulished version (APA):
Sigmund, P., Osmani, O., & Schinner, A. (2014). Anatomy of charge-exchange straggling. *Nuclear Instruments and Methods in Physics Research Section B: Beam Interactions with Materials and Atoms*, *338*, 101-107. https://doi.org/10.1016/j.nimb.2014.08.006

Anatomy of Charge-Exchange Straggling

P. Sigmund[a], O. Osmani[b], A. Schinner[c]

[a]*Department of Physics, Chemistry and Pharmacy, University of Southern Denmark, DK-5230 Odense M, Denmark*
[b]*Department of Physics, University of Duisburg-Essen, D-47048 Duisburg, Germany*
[c]*Institut für Experimentalphysik, Johannes Kepler Universität, A-4040 Linz, Austria*

Abstract

We have studied charge-exchange straggling theoretically for swift krypton and silicon ions and five target gases in the MeV/u energy regime. We find a pronounced two-peak structure for all ion-target combinations. The peak at the highest energy appears around the velocity where the bare ion and the one-electron ion are equally abundant in the equilibrium charge distribution. Correspondingly, the low-energy peak appears near the cross-over between the charge fractions of the two- and the three-electron ion. Stimulated by an experimental result, the possible existence of a third peak is discussed.

Keywords: Stopping power, Straggling, Charge exchange, Charge equilibrium, Swift heavy ions
PACS: 34.10.+x, 34.50.Bw, 34.50.Fa, 34.70.+e, 52.40.Mj, 61.85.+p

July 17, 2014

1. Introduction

Charge exchange is an important component in the understanding of the penetration of swift ions through matter [1]. Electron capture and loss by the penetrating ion affect the mean energy loss and, especially, the energy-loss fluctuation (straggling), where at least two aspects need consideration,

- the energy transfer between the ion and the medium in a capture or loss process, and
- the variation in the mean energy loss between different charge states of the ion.

Based on early work of Vollmer [2], Efken et al. [3] and Winterbon [4], a general statistical theory of charge-exchange straggling has been developed [5, 6] which, subsequently, has focused on the case of charge equilibrium [7] and has recently been applied in the analysis of experiments [8].

Charge-exchange straggling depends on the ion-target combination and on the beam energy, and since there are other processes that contribute to straggling [1, 9], frequently summarized under the heading 'collisional straggling', it is not a trivial task to separate the two processes experimentally. Based on early experiments [3, 10, 11] and a well-known formula for a two-state system [3], it has been commonly assumed that the dependence of charge-exchange straggling on energy is bell-shaped and superimposed on the contribution from collisional straggling which is tasken to be rather constant except at low projectile speeds. This view has been condensed in a frequently-used empirical interpolation formula by Yang et al. [12].

The present study focuses on two main aspects:

Email address: sigmund@sdu.dk (P. Sigmund)

- Identifying trends regarding the magnitude and relative significance of charge-exchange straggling as a function of the ion and target species.
- Our previous theoretical analysis [8] gave indications of a double-peak structure in the energy dependence. Since collisional straggling alone also may lead to at least a single-peak structure due to packing and bunching [13], it is desirable to develop tools to classify such peaks.

We have attacked these problems within available theory. Much can be learned from mere inspection of the two-state case based on the Efken formula [3] and its extended version [5].

2. Recapitulation

Following refs. [5, 13] we operate with three parameters,

$$\sigma_{IJ} = \int d\sigma_{IJ}(T), \tag{1}$$

$$S_{IJ} = \int T\, d\sigma_{IJ}(T), \tag{2}$$

$$W_{IJ} = \int T^2\, d\sigma_{IJ}(T), \tag{3}$$

where $d\sigma_{IJ}(T)$ denotes the differential cross section for energy transfer (T, dT) in a collision where the state of the projectile changes from I to J. The terminology 'state' denotes most often a charge state but may also include an excitation state. If the former, σ_{IJ} denotes cross sections for single and multiple electron capture and loss, S_{IJ} denotes partial stopping cross sections entering the mean energy loss, and W_{IJ} is one of the ingredients in straggling.

We also need charge fractions $F_{IJ}(x)$, which denote the probability for a projectile to be in state J after a penetration depth x if it was in state I at $x = 0$. In case of (charge) equilibrium this quantity reduces to $F_{IJ}(\infty) = F_J$.

Finally we need state-dependent stopping cross sections and straggling parameters,

$$S_I = \sum_J S_{IJ}, \tag{4}$$

$$W_I = \sum_J W_{IJ}, \tag{5}$$

which do not differentiate between final states.

With this, the mean energy loss per pathlength x reads

$$\left(\frac{d\langle\Delta E\rangle}{Ndx}\right)_I = \sum_J F_{IJ}(x) S_J, \tag{6}$$

and the fluctuation,

$$\frac{d}{Ndx}\left(\left\langle\Delta E^2\right\rangle_I - \langle\Delta E\rangle_I^2\right) = \sum_J F_{IJ}(x) W_J + \left(\frac{d\Omega^2}{Ndx}\right)_I, \tag{7}$$

where [5]

$$\left(\frac{d\Omega^2}{Ndx}\right)_I = 2\sum_{JKL} N \int_0^x dx'\, F_{IJ}(x - x') S_{JK} \left[F_{KL}(x') - F_{IL}(x)\right] S_L, \tag{8}$$

and N denotes the number of target particles (atoms or molecules) per volume.

In the following we focus on charge equilibrium, $x \to \infty$, where

$$\left(\frac{d\langle\Delta E\rangle}{Ndx}\right)_I \to \frac{d\langle\Delta E\rangle}{Ndx} = \sum_J F_J S_J, \tag{9}$$

and [13]

$$\left(\frac{d\Omega^2}{Ndx}\right)_I \to \frac{d\Omega^2}{Ndx} = 2N \sum_{JKL} F_J S_{JK} S_L \int_0^\infty dx \, [F_{KL}(x) - F_L] \,. \tag{10}$$

3. The Two-state Case

If there are only two or three states, analytical expressions exist for the charge fractions $F_{IJ}(x)$ [14]. For the two-state case one finds

$$F_1 = \frac{\sigma_{21}}{\sigma}; \qquad F_2 = \frac{\sigma_{12}}{\sigma}, \tag{11}$$

where $\sigma = \sigma_{12} + \sigma_{21}$. The straggling then reduces to [5]

$$\frac{d\Omega^2}{Ndx} = \left(\frac{d\Omega^2}{Ndx}\right)_{\text{coll}} + \left(\frac{d\Omega^2}{Ndx}\right)_{\text{chex}}, \tag{12}$$

where

$$\left(\frac{d\Omega^2}{Ndx}\right)_{\text{coll}} = \frac{1}{\sigma} \left(\sigma_{21} W_1 + \sigma_{12} W_2\right) \tag{13}$$

and

$$\left(\frac{d\Omega^2}{Ndx}\right)_{\text{chex}} = \frac{2}{\sigma^3} \left(S_1 - S_2\right) \left[\left(\sigma_{21} S_{11} + \sigma_{12} S_{21}\right) \sigma_{12} - \left(\sigma_{21} S_{12} + \sigma_{12} S_{22}\right) \sigma_{21}\right] . \tag{14}$$

Eq. (14) can be written in a more transparent form,

$$\left(\Delta\Omega^2\right)_{\text{chex}} = \frac{2F_1F_2}{Nx\sigma} \left(\epsilon_1 - \epsilon_2\right)^2 - \frac{2}{Nx\sigma} \left(\epsilon_1 - \epsilon_2\right) \left(F_1\epsilon_{12} - F_2\epsilon_{21}\right) , \tag{15}$$

where

$$\epsilon_{12} = NxS_{12} \tag{16}$$

and similarly for corresponding terms[1]. If energy loss in charge exchange is neglected, $S_{12} = S_{21} = 0$, eq. (15) reduces to the wellknown formula by Efken et al. [3].

Consider the first term on the right-hand side of eq. (15):

- $\epsilon_1 - \epsilon_2$ represents the difference between the mean energy losses in states 1 and 2. Clearly, fluctuations are large if this quantity is large.
- $Nx\sigma$ represents the mean number of capture-loss cycles during a passage. Fluctuations decrease if this quantity increases.
- Most interesting is the factor F_1F_2, which has a maximum for $F_1 = F_2 = 1/2$, since $F_1 + F_2 = 1$.

Regarding the dependence on beam energy, mean energy losses go through a broad maximum, while the cross section for a capture-loss cycle tends to decrease more or less monotonically except at very low beam energies. As we shall see below, it is the factor F_1F_2 that primarily defines maximum charge-exchange straggling as a function of the beam energy.

[1]We have changed notation from $N\,dx$ to Nx here, keeping the pathlength x finite but small enough so that the relative energy loss $\Delta E/E \ll 1$.

4. Continuum Approximation

In ref. [7] we showed that eq. (10) can be factorized according to

$$\frac{d\Omega^2}{Ndx} = 2Ns_1 s_1' G_0, \tag{17}$$

where

$$G_0 = \sum_J F_J(q_J - q)\beta_J, \tag{18}$$

$$\beta_J = \sum_K q_K \int_0^\infty dx\ [F_{JK}(x) - F_K] \tag{19}$$

and

$$s_1 = \left(\frac{dS}{dq_J}\right)_{q_J=q}. \tag{20}$$

In eq. (20), q_J denotes an ion charge and q the mean equilibrium charge at a given projectile speed. The quantity s_1', defined in ref. [7], reduces to s_1 when energy loss in charge exchange can be neglected. An example where this approximation is not justified is discussed in section 10.

Eq. (17) is based upon the assumption that the stopping cross section S_J depends smoothly on the ion charge q_J, so that a derivative dS_J/dq_J becomes a meaningful quantity. In the limit of the two-state case, eq. (17) reduces to the exact result, eq. (15).

Eq. (17) is interesting, because the factor G_0 represents the role of charge exchange, while the factor $s_1 s_1'$ represents stopping cross sections.

5. Charge Exchange

In ref. [7], two procedures were discussed for determining the quantity G_0. In subsequent [8] as well as the present work we only employed the ETACHA code [15] which incorporates a fairly comprehensive set of atomic input parameters, allowing not only for capture and loss but also excitation as well as radiative and nonradiative decay. A weak point of this code is numerical stability, a point that is crucial in the evaluation of the quantity β_J, eq. (19). This has led to questionable results in our first applications [7]. We have tried to minimize computational errors by a slight modification of the code and, more important, by careful inspection of all functions $F_{IJ}(x)$ entering the evaluation of β_J. At the same time a code was written to compute G_0, once all relevant β_J have been found.

Figure 1 shows a comparison between the results of our previous and the present procedure. Most of all, we are now able to supply a much tighter grid of data points. There are minor discrepancies at the low-energy end and more pronounced discrepancies at the upper end. There is clear evidence for the existence of two maxima, although the position of the low-energy maximum appears to lie below the lower energy limit of the ETACHA code.

Figure 2 shows G_0 for Kr in He, N_2, Ne, Ar and Kr. Here the low-energy peak is clearly seen for all target gases except helium. Both peaks tend to move to higher energies with increasing atomic number of the target. While the height of the high-energy peak decreases with increasing target mass, a systematic behavior of the height of the low-energy peak is not visible in the graph. While it is conceivable that a third maximum exists at even lower energies, the ETACHA code does not allow us to run at energies below those shown in figure 2.

Figure 3 shows similar data for Si ions. While qualitative trends are the same, the height of the high-energy peak appears to go through a minimum for a Ne target.

6. Shima Plot

Figure 4 shows equilibrium charge fractions F_J for Kr ions versus beam energy according to ETACHA, plotted similarly to those in the tables by Shima et al. [16]. The two graphs look similar on first sight, as do the ones for N_2, Ne and Ar target gases that are not shown. The same holds true for figure 5 which shows the corresponding graphs for Si ions.

Consider first figure 4 for Kr ions. At the highest energies, bare ions are most abundant. Going to lower energies there is a cross-over between F^{36+} and F^{35+} at an energy $E^{(01)}$. Approximating the energy interval around $E^{(01)}$ as a two-state system, one expects maximum charge-exchange straggling here. Table 1 shows that indeed, G_0 has a maximum at an energy $E_{\mathrm{high,max}}$ slightly below $E^{(01)}$. The small difference is asserted to be due to interference with the two-electron state 34+ which has a charge fraction between 0.13 and 0.17 in the cross-over $E^{(01)}$ for the systems listed, as is seen in the last column of table 1.

Figure 5 shows very similar features for Si ions if the comparison is done between ions with equal numbers of bound electrons.

The Shima plots in figures 4 and 5 reveal a wide energy region dominated by the two-electron ion, where charge-exchange straggling should be relatively small on the basis of our analysis of the two-state case. Indeed, G_0 is seen to go through a minimum in all curves in figures 2 and 3 at an energy $E_{\mathrm{min}}^{(G_0)}$ listed in the fourth column in figure 1. Following the above argument, one would expect a maximum of G_0 at the cross-over $E^{(23)}$ between F^{34+} and F^{33+} for Kr, and F^{12+} and F^{11+} for Si. Table 1 shows that the low-energy maximum that is found in figures 2 and 3 lies below $E^{(23)}$ as expected, but the relative difference is greater than in case of the high-energy maximum. This must be expected in view of the vicinity of a larger number of contributing charge states. This is also asserted to be the cause of the decrease in height as compared to the high-energy maximum.

This analysis suggests more peaks at lower beam energies, although it is not obvious whether they can be resolved. Calculations for lower beam energies and/or higher-Z_1 ions are necessary to study this point. Pronounced charge-exchange straggling has indeed been found experimentally for up to 1000 MeV/u bismuth ions [17].

7. Stopping

Charge-dependent stopping cross sections used in the following have been found from the PASS code [18, 19] with input parameters from ref. [20]. Frozen-charge stopping cross sections were computed for three charges around the mean equilibrium charge, and derivatives dS/dq were found by fitting a parabola through these three points. Figure 6 shows results for Kr ions. In the energy interval covered, all curves decrease monotonically with increasing energy.

Only target excitation and ionization have been taken into account, while energy transfer in electron capture and loss has been ignored, in accordance with the conventional procedure [3, 11]. This approximation is discussed in section 10.

8. Results

Figures 7 and 8 show calculated charge-exchange straggling, normalized to Bohr straggling

$$\frac{d\Omega^2_{\mathrm{Bohr}}}{N dx} = 4\pi Z_1^2 Z_2 e^4 \tag{21}$$

for Kr and Si ions in five targets. In comparison with figures 2 and 3, maxima have shifted toward smaller energies due to the monotonic decrease of dS/dq. For the same reason, low-energy maxima have become relatively more pronounced.

Figure 9 shows calculated straggling for krypton ions, normalized to Bohr straggling. Curves labeled 'Total' include linear straggling, bunching and packing determined by the PASS code. Here, linear straggling denotes the sum of the fluctuations in the energy loss to single target electrons [21], while bunching and packing denote correlations. Bunching takes into account the spatial confinement of the electrons in a target atom [11], while packing represents the spatial proximity of the two nitrogen atoms in a molecule [22]. These three effects were evaluated as s described in refs. [13, 21]. Also included are experimental results by Vockenhuber et al. [8].

It is seen that charge exchange is the dominating contribution to straggling for Kr-He up to ~ 100 MeV/u. Conversely, for Kr-Kr, the dominating contribution is bunching up to ~ 30 MeV/u and linear straggling at higher energies, yet charge-exchange straggling is high enough for Kr-Kr to generate a visible high-energy peak. The position of the low-energy peak coincides with the bunching peak, which yields the major contribution to the the total.

The magnitude of the ratio $\Omega^2/\Omega^2_{\rm Bohr}$ is found to decrease by about two orders of magnitude from Kr-He to Kr-Kr. This behavior is mostly due to the charge-exchange constribution: On an absolute scale this is related to the quantity s_1 shown in figure 6 which enters eq. (17) in the second power. On a relative scale one may note that $\Omega^2_{\rm Bohr}$, in contrast to $\Omega^2_{\rm chex}$ is proportional to Z_2.

9. Discussion

Figure 9 includes experimental data from an experiment reported in ref. [8] but based on a revised data analysis performed by C. Vockenhuber (private communication) and to be specified in a forthcoming publication [23].

The comparison of experimental data with the calculations reveals some trends:

- Theory appears to overestimate straggling for Kr-He und to underestimate straggling for Kr-Kr, while fairly good agreement is found for Kr-N_2 and Kr-Ne.
- None of the experimental data sets overlaps the regime of the high-energy peak. This was the motivation for initiating experiments with Si ions [23].
- For Kr-He and Kr-Ne, and possibly also for Kr-N_2, theoretical curves appear shifted by 30-40 % toward higher energies compared with the experimental data.

We see at least two reasons for the observed discrepanices between theory and experiment:

1. On the theoretical side the dominating uncertainty originates in the ETACHA code. Apart from numerical instabilities – which we have tried our best to minimize – work by Imai et al. [24, 25] shows significant discrepancies between calculated and measured results for the evolution of the mean charge state, the quantity that enters our β_J parameters, eq. (19). In our evaluation of S-C data, figure 6 in ref. [26], ETACHA underestimates the tails in the transients at large depths as well as the aproach to equilibrium in the initial stage. This difference may be substantial and may affect both the magnitude and the energy dependence of the parameters β_J which enter charge-exchange straggling in the first power.
   We note that the lower end of the energy range covered in the five curves in figure 7 is determined by the ETACHA code: Any attempt to go to lower energies caused a crash of the program. This appears indicative of significant error bars of the output near the apparent threshold. This also sets a question mark at the high predicted value of charge-exchange straggling in Kr-He at the low-energy end (figure 7).

2. For Kr-Kr, bunching is an important contribution to straggling. Our calculation of bunching, based on an independent-electron target atom [13], appears to underestimate the height and to overestimate the position of the peak. The prime quantity entering the model is the impact-parameter dependence of the mean energy loss. No independent tests are available on the validity of our approach for such a heavy collision system at relatively low energies.

While discrepancies observed for Kr-He and Kr-Kr are clearly unsatisfactory, we find the agreement in case of Kr-N_2 and Kr-Ne encouraging. Moreover, we have arrived at theoretical guidelines for experimental studies of one, two and possibly more maxima in the energy-loss straggling.

10. Note on Kr-Kr

As noted above, the present treatment, based on the ETACHA code, does not allow us to quantitatively study the energy regime where figure 9 seems to indicate a major discrepancy between calculated and measured straggling for the Kr-Kr system. To see what is going on, have a look at figure 4, lower graph, which indicates two important crossings at energies $E^{(01)}$ and $E^{(23)}$ listed in table 1. Now, at the low-energy end the charge fraction F^{26+}, representing a filled L shell, is seen to reach a level above 0.5 and, moreover, F^{25+}, representing a Na-like ion, is well separated in energy from F^{26+} in energy. This is indicative of a straggling peak comparable with the high-energy peak and more pronounced than what we identified as the low-energy peak for the other targets. If so, this third peak is expected to be located at an energy below 8 MeV/u, which appears compatible with the observations.

Considering the fact that the two peaks in the calculated energy dependence of charge-exchange straggling lie at least an order of magnitude below the observations, one might question whether an evaluation of G_0 would be sufficient for achieving an adequate estimate. Here we argue that it is not.

The energy loss in charge-changing collisions is generally acknowledged as a contribution to the mean energy loss. It is also included explicitly or implictly in codes and tabulations of stopping cross sections such as ref. [20]. The effect has commonly been ignored in explicit estimates of charge-exchange straggling, but it has been included in the formalism developed in ref. [5] as well as in studies of multiple-peak energy-loss spectra by Ogawa et al. [27].

Figure 10 shows the relative importance of projectile processes in equilibrium stopping. The PASS code delivers separate output for target excitation/ionization, S_{TE}, on the one hand and projectile excitation, electron capture and loss on the other, summarized as $S_{\rm PE}$. Plotted is the ratio $S_{\rm PE}/\left(S_{\rm TE}+S_{\rm PE}\right)$. It is seen that this contribution is significant at least in the lower half of the covered energy range, in decreasing order from Kr to He targets, and that it diminishes rapidly above 10 MeV/u.

Figure 11 shows a comparison between $S_{\rm coll}$, the collisional stopping cross section disregarding projectile processes, and quantities that enter the contributions to the stopping cross section from electron capture and loss. All results refer to charge equilibrium, so the same number was chosen for the cross sections for capture and loss. Loss cross sections were calculated by PASS [28]. It is common to set the energy loss in a capture event to

$$T_{\rm capt} \simeq mv^2/2 + U_2 - U_1 \tag{22}$$

and in a loss event to

$$T_{\rm loss} \simeq U_1, \tag{23}$$

where U_1 and U_2 are binding energies of projectile and target, respectively, dependent on the shells involved.

Figure 11 shows the contributions from $mv^2/2$ and various binding energies separately. It is seen that $\sigma_M mv^2/2$ dominates for both Kr-He and Kr-Kr, but while it is almost an order of magnitude smaller than $S_{\rm coll}$ in case of Kr-He, it exceeds $S_{\rm coll}$ significantly in case of Kr-Kr. However, $\sigma_M mv^2/2$ is only relevant when the L shell is occupied, i.e., below ~ 5 MeV/u. Above that energy one expects a gradual transition into parameters characterizing the L shell which are significantly lower. Quantities characterizing the K shell are insignificant on the scale of the graph.

Clearly, an evaluation of charge-exchange straggling at least for the Kr-Kr system requires going beyond the Vollmer scheme, where energy loss in charge-changing collisions is neglected. This may involve dropping the continuum approximation developed in ref. [7] and going back to the comprehensive formulation in ref. [5].

Acknowledgements

We like to thank Christof Vockenhuber for performing an improved analysis of the experimental data reported in ref. [8]. We are grateful to D. Vernhet and J. P. Rozet for kindly making available their ETACHA code. This work has been supported by the Carlsberg Foundation.

References

[1] P. Sigmund, *Particle Penetration and Radiation Effects Volume 2*, vol. 179 of *Springer Series in Solid State Sciences* (Springer, Heidelberg, 2014).

[2] O. Vollmer, Nucl. Instrum. Methods 121 (1974) 373.

[3] B. Efken, D. Hahn, D. Hilscher and G. Wüstefeld, Nucl. Instrum. Methods 129 (1975) 219.

[4] K. B. Winterbon, Nucl. Instrum. Methods 144 (1977) 311.

[5] P. Sigmund, Nucl. Instrum. Methods B 69 (1992) 113.

[6] A. Närmann and P. Sigmund, Phys. Rev. A 49 (1994) 4709.

[7] P. Sigmund, O. Osmani and A. Schinner, Nucl. Instrum. Methods B 269 (2011) 804.

[8] C. Vockenhuber, J. Jensen, J. Julin, H. Kettunen, M. Laitinen, M. Rossi, T. Sajavaara, O. Osmani, A. Schinner, P. Sigmund and H. J. Whitlow, Europ. Phys. J. D 67 (2013) 145.

[9] P. Sigmund, *Particle penetration and radiation effects*, vol. 151 of *Springer Series in Solid-State Sciences* (Springer, Berlin, 2006).

[10] C. J. Sofield, N. E. B. Cowern, R. J. Petty, J. M. Freeman and J. P. Mason, Phys. Rev. A 17 (1978) 859.

[11] F. Besenbacher, J. U. Andersen and E. Bonderup, Nucl. Instrum. Methods 168 (1980) 1.

[12] Q. Yang, D. J. O'Connor and Z. Wang, Nucl. Instrum. Methods B 61 (1991) 149.

[13] P. Sigmund and A. Schinner, Europ. Phys. J. D 58 (2010) 105.

[14] S. K. Allison, Rev. Mod. Phys. 30 (1958) 1137.

[15] J. P. Rozet, C. Stephan and D. Vernhet, Nucl. Instrum. Methods B 107 (1996) 67.

[16] K. Shima, N. Kuno, M. Yamanouchi and H. Tawara, Atom. Data Nucl. Data Tab. 51 (1992) 173.

[17] H. Weick, H. Geissel, C. Scheidenberger, F. Attallah, T. Baumann, D. Cortina, M. Hausmann, B. Lommel, G. Münzenberg, N. Nankov, F. Nickel, T. Radon, H. Schatz, K. Schmidt, J. Stadlmann, K. Sümmerer, M. Winkler and H. Wollnik, Nucl. Instrum. Methods B 164-165 (2000) 168.

[18] P. Sigmund and A. Schinner, Europ. Phys. J. D 12 (2000) 425.

[19] P. Sigmund and A. Schinner, Nucl. Instrum. Methods B 195 (2002) 64.

[20] ICRU, *Stopping of ions heavier than helium*, vol. 73 of *ICRU Report* (Oxford University Press, Oxford, 2005).

[21] P. Sigmund and A. Schinner, Europ. Phys. J. D 23 (2003) 201.

[22] P. Sigmund, Phys. Rev. A 14 (1976) 996.

[23] C. Vockenhuber, M. Thöni, J. Jensen, K. Arstila, J. Julin, H. Kettunen, M. Laitinen, M. Rossi, T. Sajavaara, H. J. Whitlow, O. Osmani, A. Schinner and P. Sigmund, in preparation (2014).

[24] M. Imai, M. Sataka, K. Kawatsura, K. Takahiro, K. Komaki, H. Shibata, H. Sugai and K. Nishio, Nucl. Instrum. Methods B 256 (2007) 11.

[25] M. Imai, M. Sataka, K. Kawatsura, K. Takahiro, K. Komaki, H. Shibata, H. Sugai and K. Nishio, Nucl. Instrum. Methods B 267 (2009) 2675.

[26] O. Osmani and P. Sigmund, Nucl. Instrum. Methods B 269 (2011) 813.

[27] H. Ogawa, I. Katayama, Y. Haruyama, F. Fukuzawa, K. Yoshida, A. Aoki, M. Tosaki, I. Sugai and H. Ikegami, Phys. Lett. A 160 (1991) 77.

[28] M. S. Weng, A. Schinner, A. Sharma and P. Sigmund, Europ. Phys. J. D 39 (2006) 209.

Table 1: Maxima $E^{(G_0)}_{\mathrm{high,max}}$, $E^{(G_0)}_{\mathrm{low,max}}$ and minimum $E^{(G_0)}_{\mathrm{min}}$ of G_0 from figures 2 and 3 compared with cross-overs $E^{(01)}$ and $E^{(23)}$ in the Shima plot, figures 4 and 5: The last column shows the charge fraction of the two-electron ion at an energy $E^{(01)}$. The number of digits in the data points does not reflect the accuracy but the chosen grid in the computations.

Target	$E^{(01)}$ [MeV/u]	$E^{(G_0)}_{\mathrm{high,max}}$ [MeV/u]	$E^{(G_0)}_{\mathrm{min}}$ [MeV/u]	$E^{(23)}$ [MeV/u]	$E^{(G_0)}_{\mathrm{low,max}}$ [MeV/u]	F^{34+}
Kr-He	20.4	19.0	5	2.5	< 1	0.14
Kr-N_2	33.0	32.5	15	12	7.5	0.15
Kr-Ne	40.6	40.0	17.5	15	8.75	0.16
Kr-Ar	56.3	55.0	22.5	19	11	0.16
Kr-Kr	71.1	70.0	30	25	15	0.16
						F^{12+}
Si-He	3.2	3.2	1.1	0.8	< 1	0.17
Si-N_2	7.5	7.5	2.25	1.9	$\lesssim 1$	0.15
Si-Ne	9.0	9.0	2.5	1.9	1.0	0.14
Si-Ar	11.4	10.0	4.0	3.1	2.0	0.13
Si-Kr	16.1	16.0	6.0	4.7	3.0	0.13

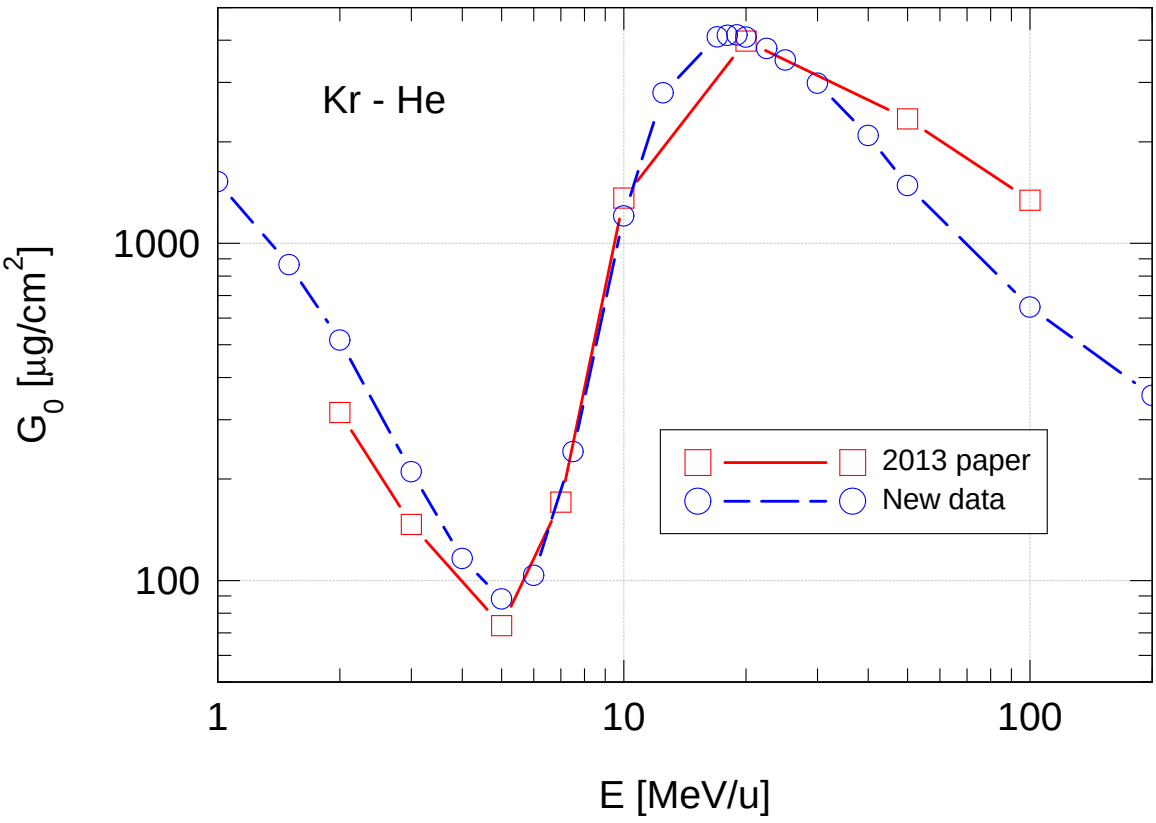

Figure 1: (Color on screen). Determination of G_0, eq. (18) from ETACHA code. 2013 paper: Input to calculations in ref. [8]. New data: Present evaluation.

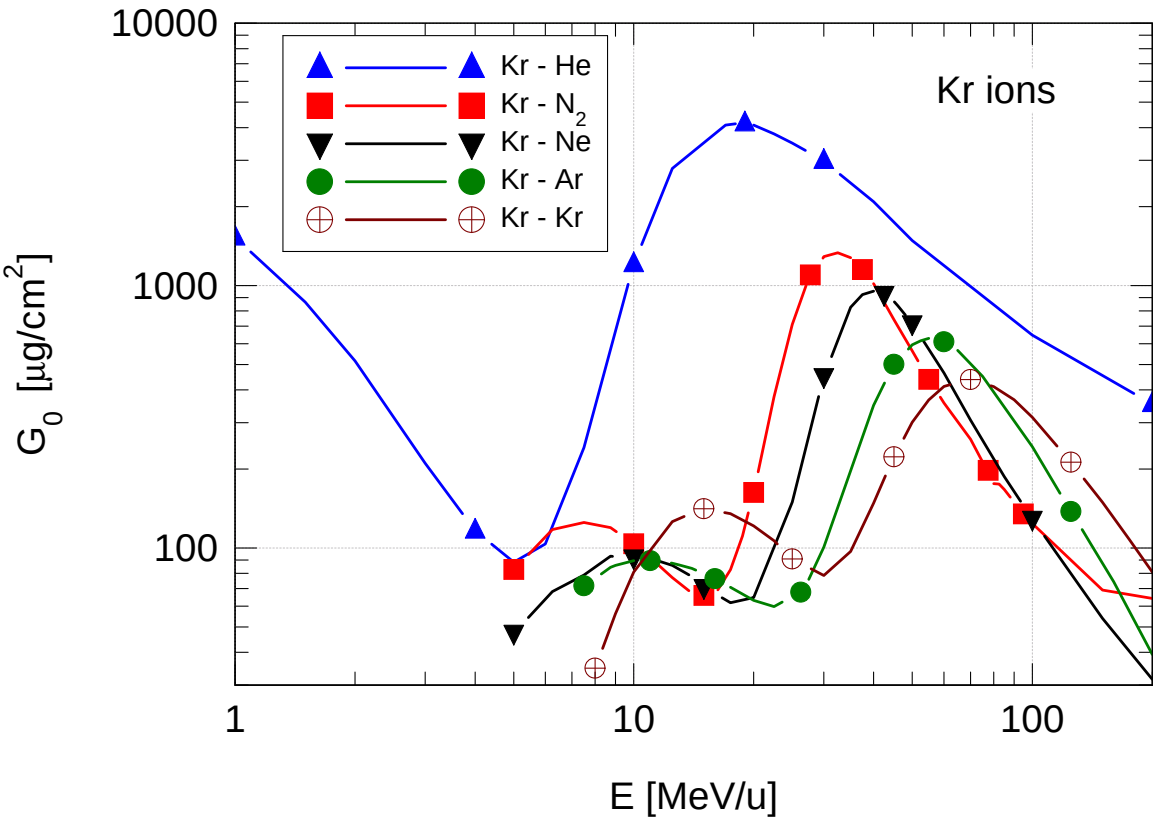

Figure 2: (Color on screen). The function G_0 versus beam energy E for Kr ions in He, N_2, Ne and Kr.

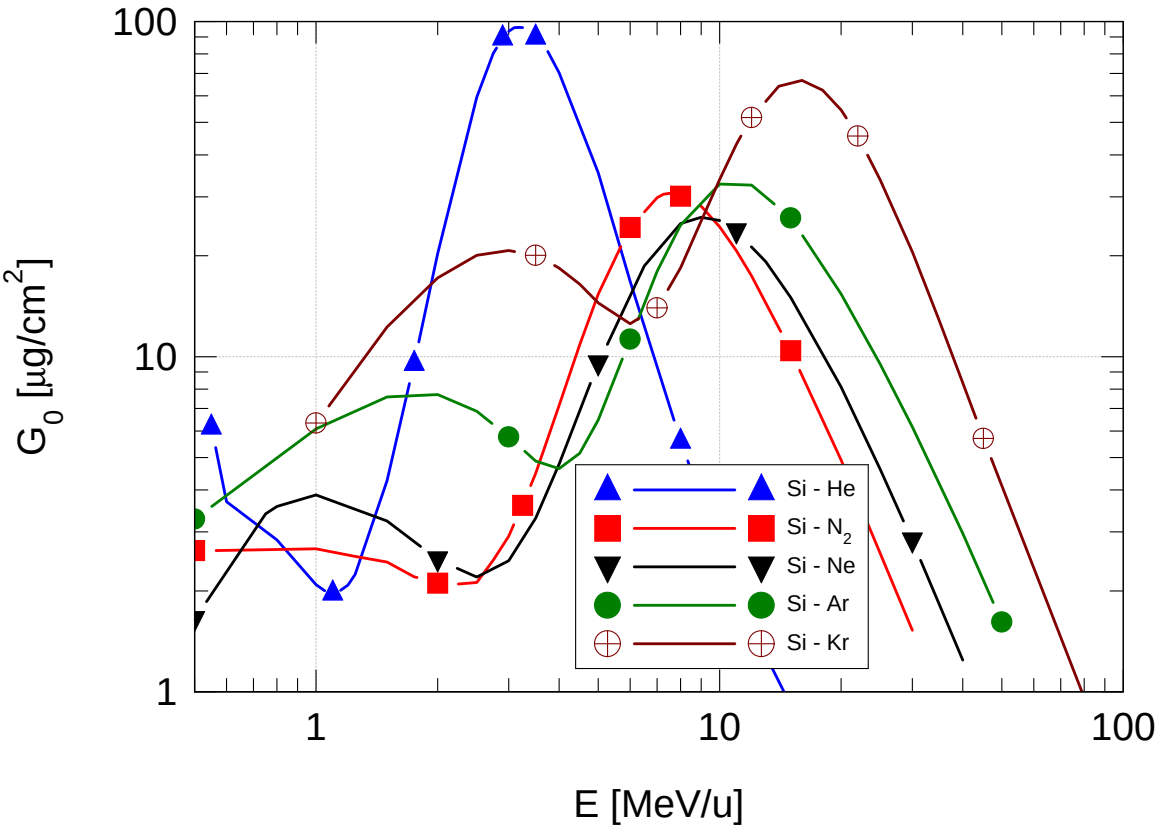

Figure 3: (Color on screen). Same as figure 2 for Si ions in He, N_2, Ne, Ar and Kr.

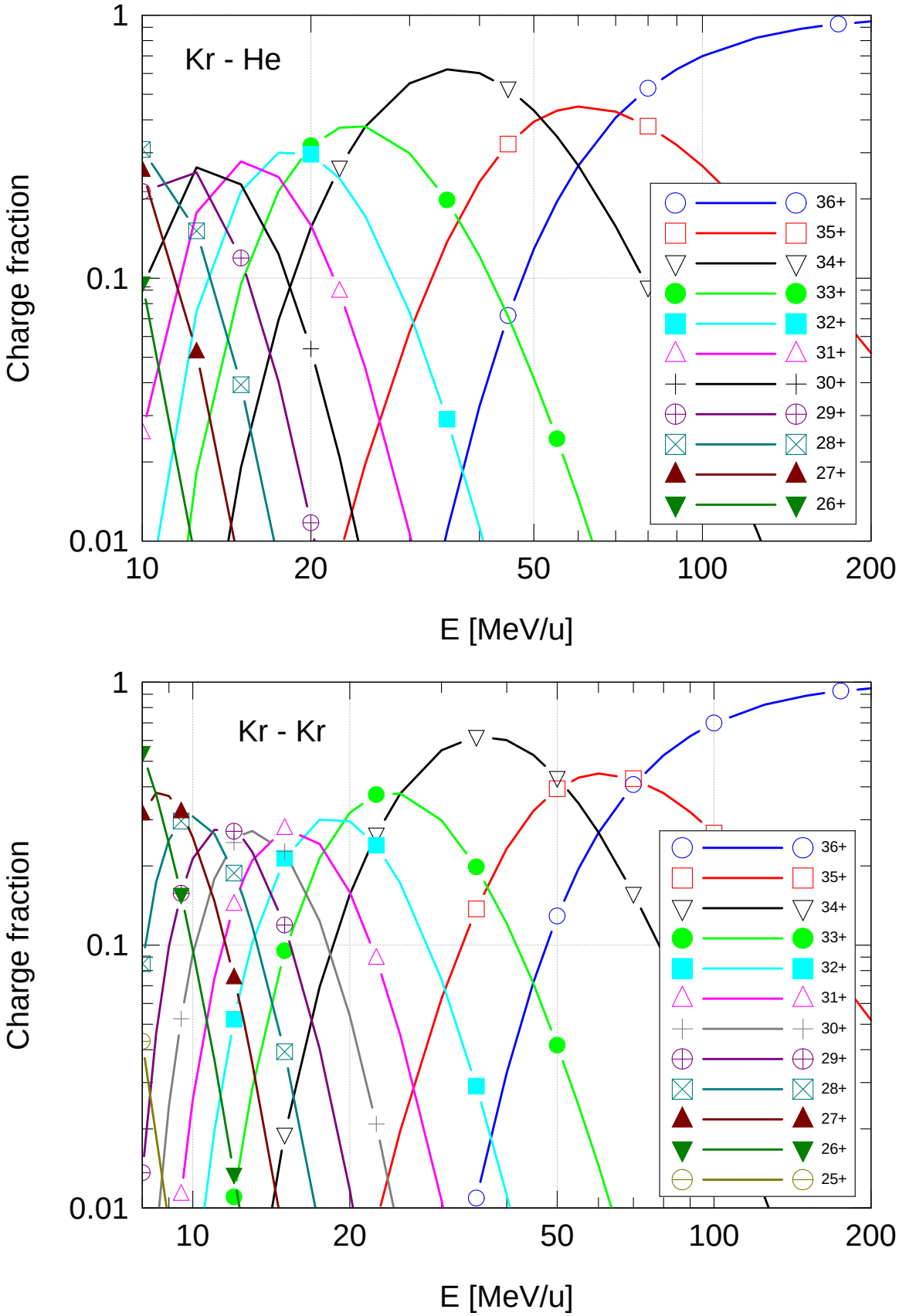

Figure 4: (Color on screen). Shima plots for Kr ions in He and Kr. Shown are the equilibrium charge fractions F_J for the highest charge states J as a function of the beam energy.

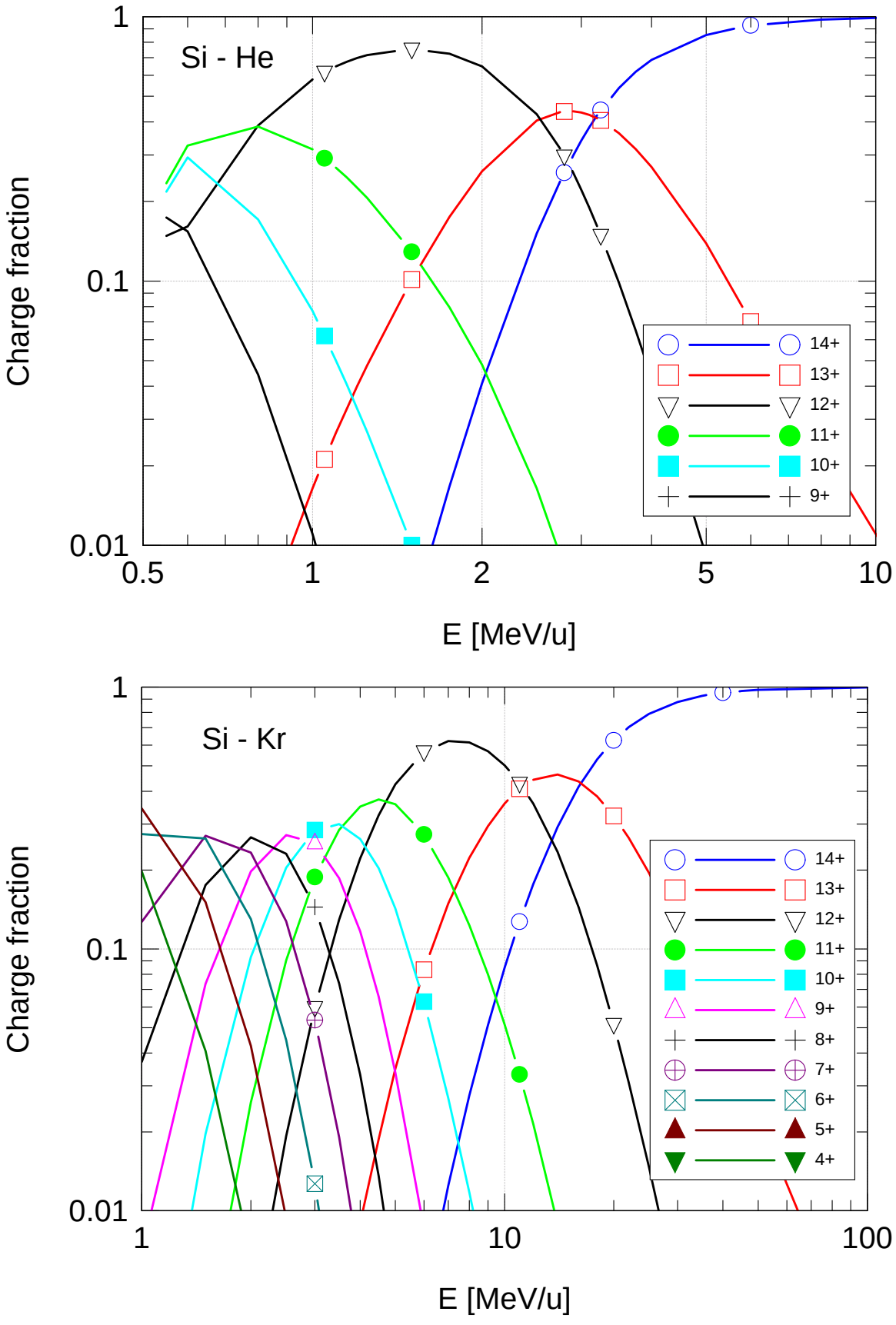

Figure 5: (Color on screen). Same as figure 4 for Si ions.

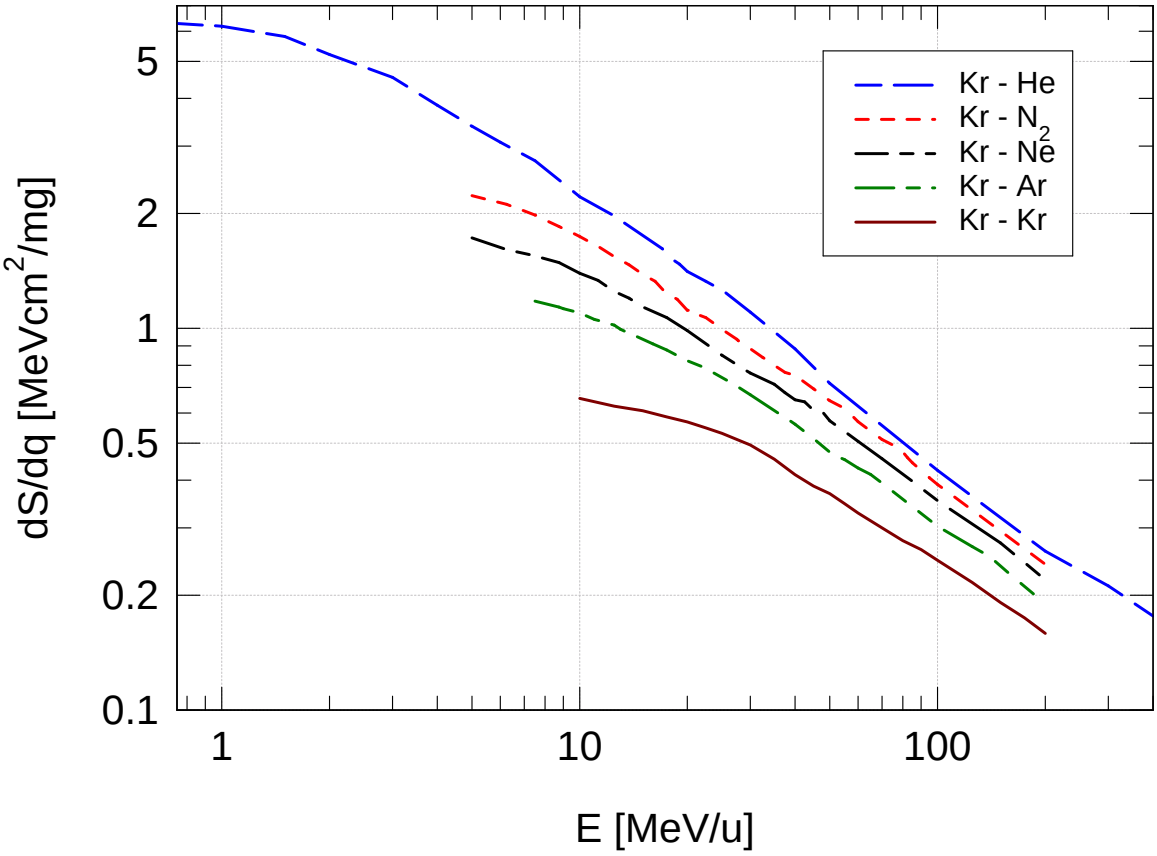

Figure 6: (Color on screen). Derivatives dS/dq at the equilibrium charge of Kr ions. Frozen-charge electronic stopping cross sections $S(q)$ from PASS code.

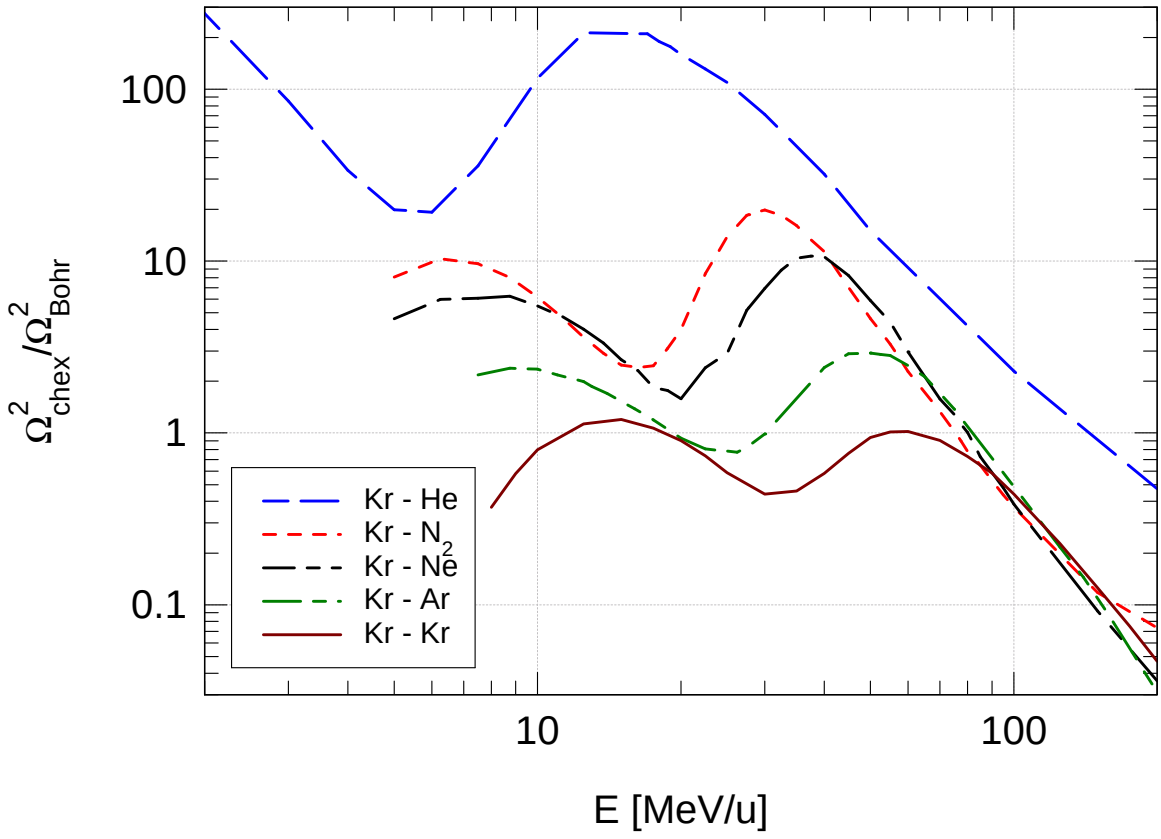

Figure 7: (Color on screen). Calculated charge-exchange straggling for Kr ions, normalized to Bohr straggling.

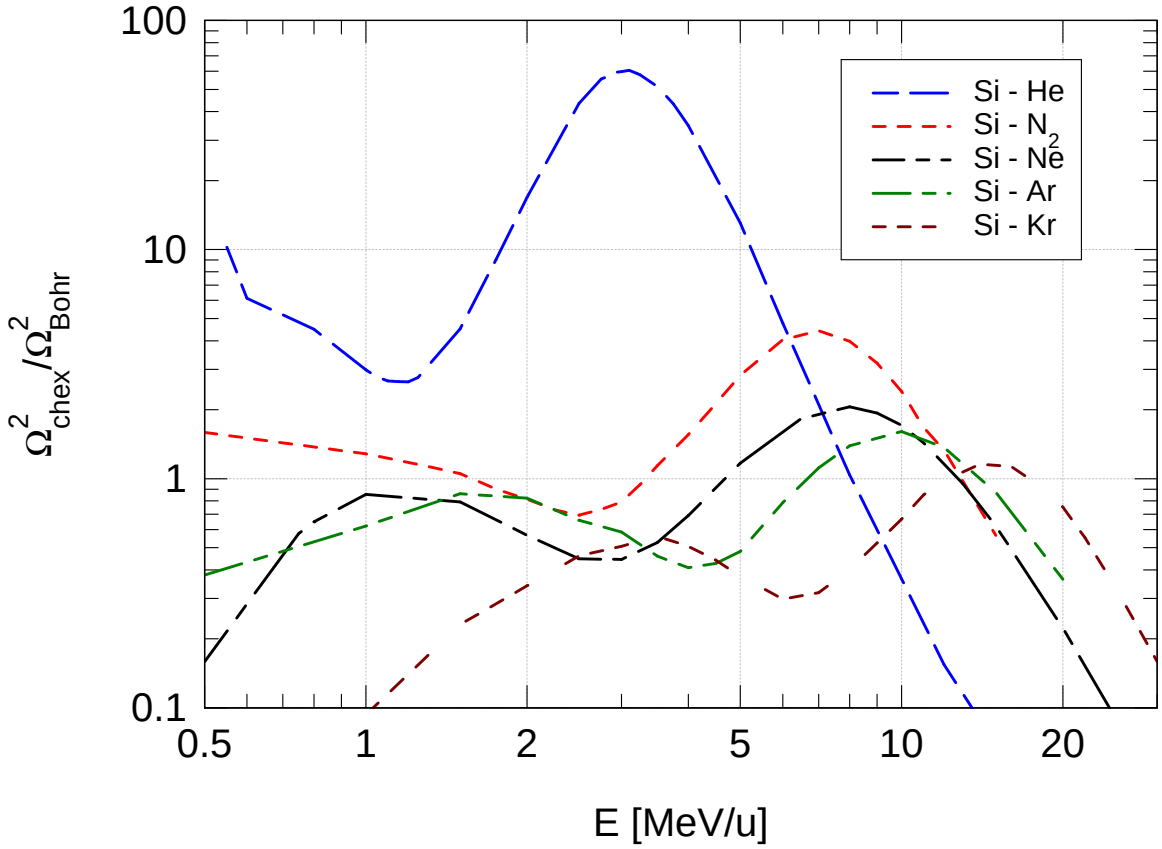

Figure 8: (Color on screen). Same as figure 7 for Si ions.

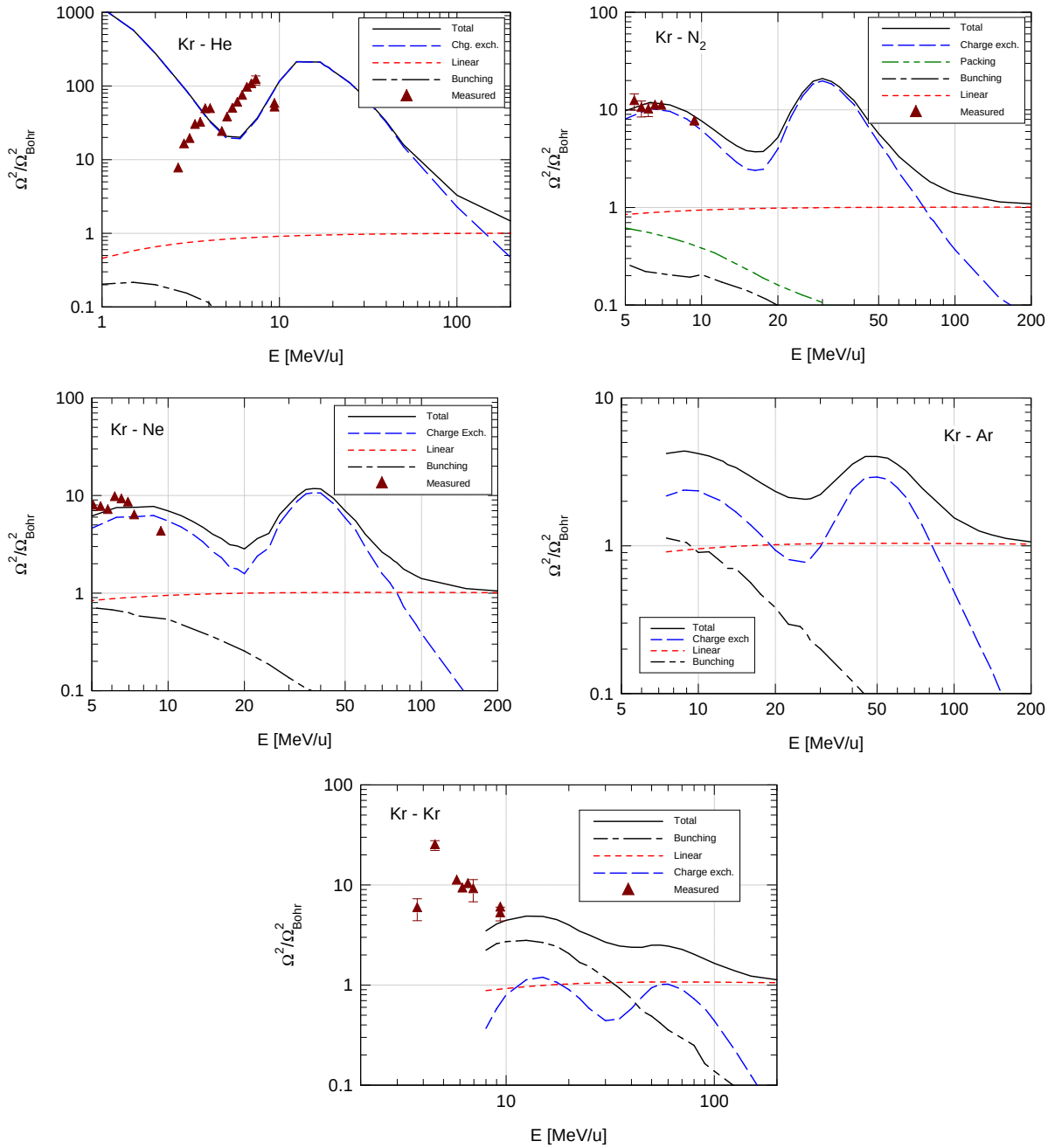

Figure 9: (Color on screen). Straggling of Kr ions normalized to Bohr straggling. Curves labeled 'Total' denote the sum of collisional and charge-exchange straggling. Collisional straggling denotes the sum of linear straggling, bunching and, in case of N_2, packing. Triangles denote experimental results of Vockenhuber et al. [8].

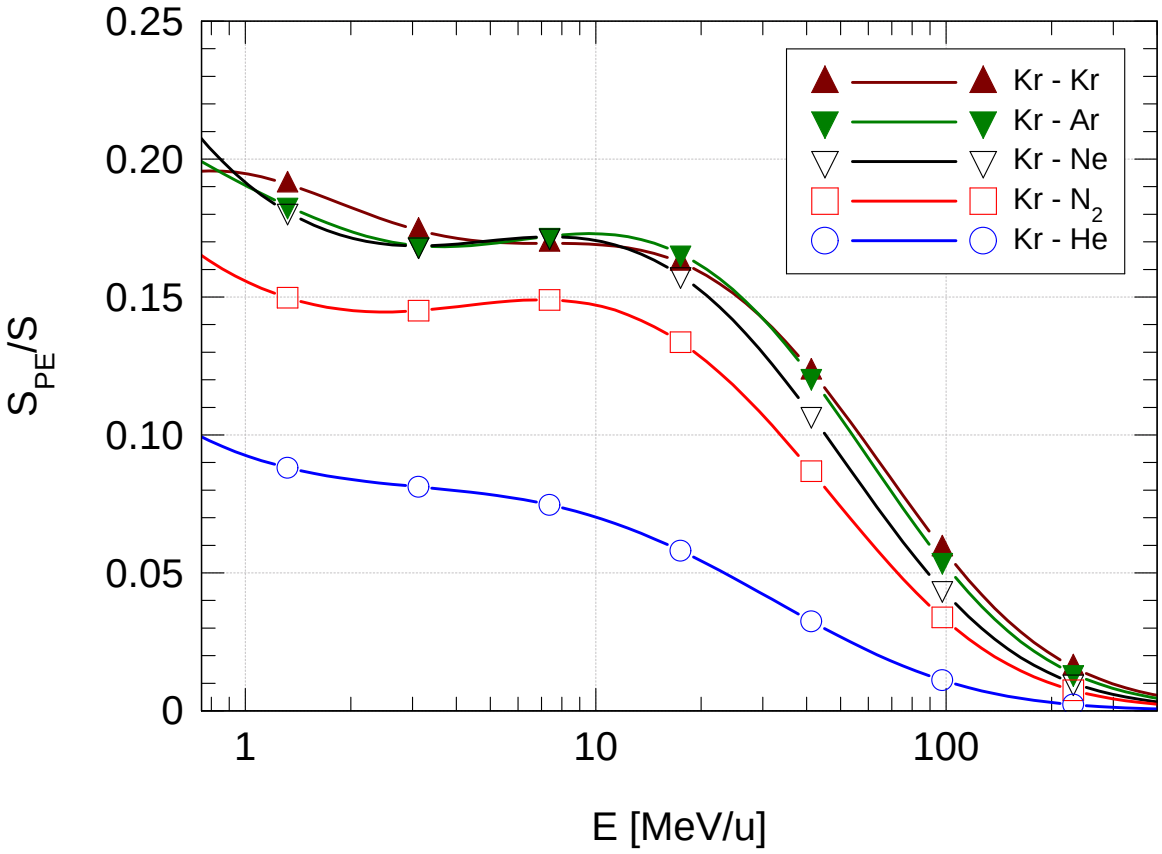

Figure 10: (Color on screen). Relative contribution of projectile processes to the stopping cross section for Kr ions in charge equilibrium. S_{PE} is the contribution of projectile excitation, electron capture and loss to the total stopping cross section S. Calculations by the PASS code [19].

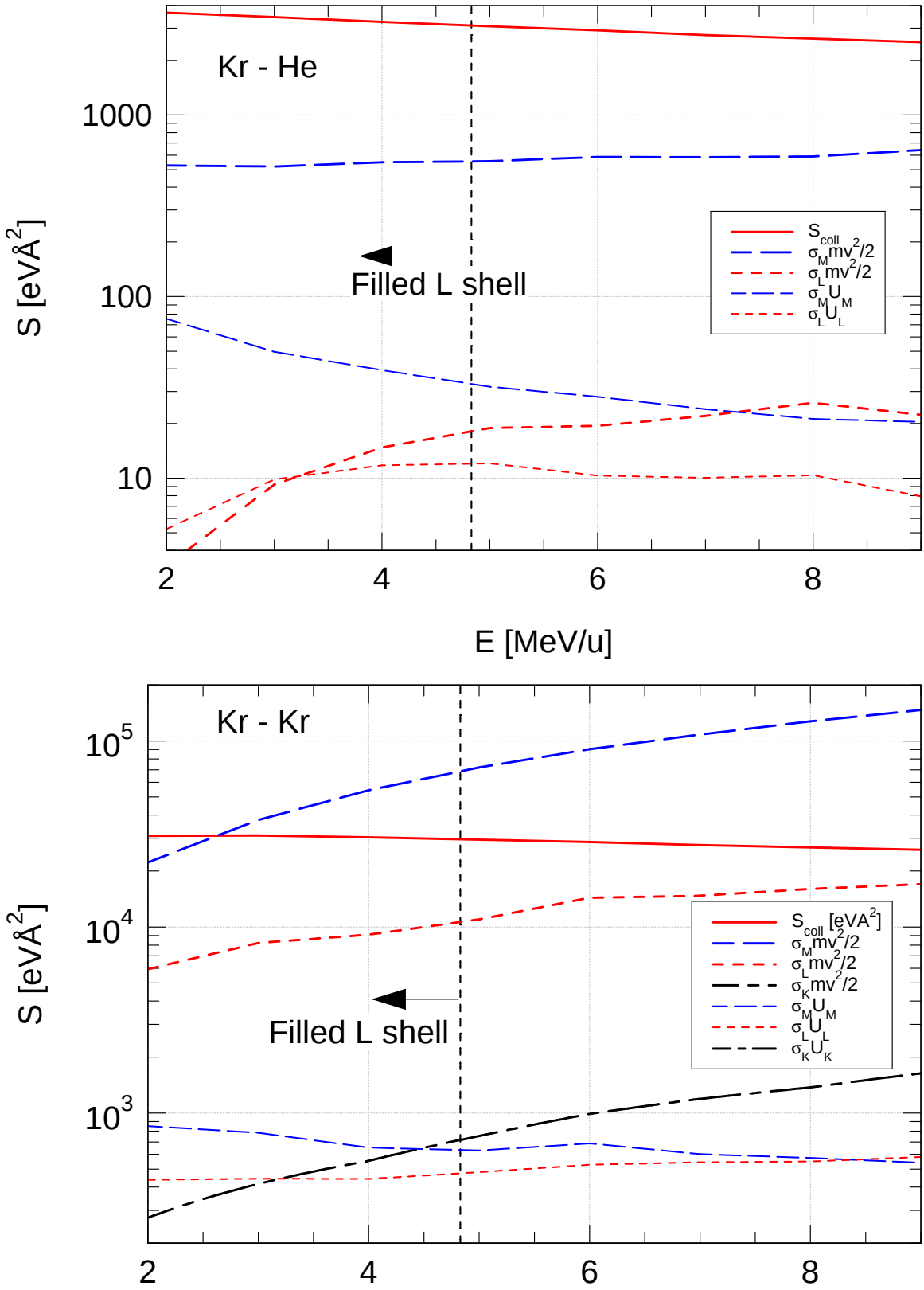

Figure 11: (Color on screen). Partial stopping cross sections for Kr-He (top) and Kr-Kr (bottom). Solid line: Collisional stopping in charge equilibrium. Broken thick lines: $\sigma_L mv^2/2$ and $\sigma_M mv^2/2$ contributing to stopping by electron into L and M states, respectively. Broken thin lines: $\sigma_L U_L$ and $\sigma_M U_M$ entering with negative sign. The corresponding quantities for K states are insignificant on the chosen scale.